Practical Variation-Aware Interconnect Delay and Slew Analysis for Statistical Timing Verification *

Xiaoji Ye
Department of ECE
Texas A&M University
College Station, TX 77843
yexiaoji@neo.tamu.edu

Peng Li
Department of ECE
Texas A&M University
College Station, TX 77843
pli@neo.tamu.edu

Frank Liu
IBM Austin Research Lab
Austin, TX 78758
frankliu@ibm.us.com

ABSTRACT

Interconnects constitute a dominant source of circuit delay for modern chip designs. The variations of critical dimensions in modern VLSI technologies lead to variability in interconnect performance that must be fully accounted for in timing verification. However, handling a multitude of inter-die/intra-die variations and assessing their impacts on circuit performance can dramatically complicate the timing analysis. In this paper, a practical interconnect delay and slew analysis technique is presented to facilitate efficient evaluation of wire performance variability. By harnessing a collection of computationally efficient procedures and closed-form formulas, process and input signal variations are directly mapped into the variability of the output delay and slew. Since our approach produces delay and slew expressions parameterized in the underlying process variations, it can be harnessed to enable statistical timing analysis while considering important statistical correlations. Our experimental results have indicated that the presented analysis is accurate regardless of location of sink nodes and it is also robust over a wide range of process variations.

1. INTRODUCTION

Interconnect parasitics are the dominant source of on-chip circuit delays for modern VLSI technologies. To account for wire delays efficiently in the design process, interconnect modeling, particularly the model order reduction of linear passive networks, has been an active topic of research in CAD community for more than one decade (e.g. [1]). The increasing interconnect performance variability [2] is also being addressed via various avenues, for instance, by variational interconnect model order reduction [3, 4], or statistical/variational interconnect analysis [5, 6].

Modern chip designs contain an overwhelmingly large number of interconnects that must be analyzed efficiently. As such, efficiency of variational interconnect analysis is critical in a statistical timing flow. The general variational reduced interconnect models do not directly offer the standard timing measures, namely, delay and slew, as well as their variability, which are needed in the existing timing analysis flows [7]. A significant cost will be incurred in order to evaluate the reduced-order models over a large number of samples to provide such delay and slew statistics. On the other hand, physical synthesis oriented delay/slew metrics [8, 9] are extremely efficient, they are not completely suitable to accurate timing verification. These metrics tend to provide inaccurate delay estimation, especially for near-end nodes in the nominal condition, making it more difficult to apply for capturing timing variability.

In this paper, we present a practical interconnect analysis methodology to provide efficient delay and slew calculation for statistical timing analysis. In our approach, process and input signal variations are translated to output delay and slew variations without extracting a "full-blown" variational reduced order model and performing subsequent sampling. While gaining improved efficiency by avoiding extracting "full-blown" models, we also develop specific techniques to avoid losing any significant accuracy in delay and slew, which is difficult to achieve via a pure delay/slew metric based approach. As a standard practice, we assume that an accurate interconnect analysis technique such as high-order AWE [1, 10] is used for the nominal timing verification, as part of a statistical timing analysis flow. Based on the result of the nominal timing analysis, each circuit node under analysis will be identified either as a "far-end" or a "near-end" node. For both, a "small-scale" parametric reduced order model will be computed. The avenue for doing so will be through fast closed-form formulas for the former and efficient perturbation analysis for the latter. It is shown that the proposed techniques offer accurate variational interconnect delay and slew computation over a wide range of process variations, regardless of the nature of circuit nodes (e.g. far ends vs. near ends). It directly produces parametric expressions of delay and slew in the underlying process variables, and hence constitutes a useful analysis infrastructure for statistical timing analysis.

2. OVERVIEW OF THE APPROACH

Given a RC network with a single voltage input, N circuit nodes and N_s sink nodes, our objective is to compute the delay $T_{d,i}$ and slew rate $T_{s,i}$ at sink node i, $i = 1...N_s$ while considering the variations of RC elements due to a set of N_ρ process variables, $\rho = [\rho_1, \rho_2, \cdots, \rho_{N_\rho}]^T$ and the voltage input variation, modeled as variation in the input slew. Without loss of generality, delay and slew are defined as 50% propogation delay and 20-80% slew time, respectively. To be accurate over a wide range of process variations, each delay is expressed in terms of a second order polynomial in process variables $\rho_i's$ as

$$T_d = T_{d,0} + \alpha_d^T \rho \ + \rho^T \Gamma_d \rho, \quad (1)$$

where T_d is the nominal delay, α_d is a $N_\rho \times 1$ vector repre-

*This work was support in part by SRC under contract 2005-TJ-1298.

ICCAD'06 November 5-9, 2006, San Jose, CA

senting the first order delay sensitivities, Γ_d is a $N_\rho \times N_\rho$ matrix representing the second order terms. For the same purpose, the second-order parametric form is used as a standard form to represent most quantities during the analysis.

The input slew can be dependent on the same or different set process parameters since it is impacted by the preceding driving stage. For simplicity of notation, we include all the process parameters in ρ. In this fashion, the statistical correlation between different circuit stages can be naturally captured. It should be noted that upon getting these parametric forms, the statistical distributions of delay and slew can be easily obtained by propagating distributions of the underlying process parameters through these quadratic expressions. As the dependency of timing quantities on process variation is kept, these parametric forms can be directly incorporated into a statistical timing analysis flow [7, 11].

The proposed analysis flow is outlined in Fig. 1. The variational interconnect analysis follows the accurate high-order AWE analysis applied for the nominal case. By examining the poles and residues of the nominal case AWE model, a sink node can be identified as a "near end" or a"far end" node. Here, a node is said to be near end if the AWE model has two obviously dominant pairs of poles and residues such that a two-pole model will be sufficient for analyzing delay and slew. Based on the parametric moment computation, parametric output slews are obtained by extending the existing moment-based nominal slew metric while considering the input slew variations [8, 9]. To more reliably compute the delay, a parametric two-pole (for "far" end nodes) or high order reduced model (for "near" end nodes) is computed. Finally, parametric forms of the delay is generated by evaluating the parametric reduced model. The efficiency of the proposed approach is archived by adopting a) an efficient variational transfer function moments computation procedure; b) a simple and yet accurate (parametric) moment-based slew metric; c) efficient closed-form formulas (far-end nodes) and numerically efficient perturbation analysis (near-end nodes) for variational delay analysis. In Fig. 1, shaded steps are performed using closed-form formulas while others are achieved using efficient numerical computation. Each of these steps is described in details as follows.

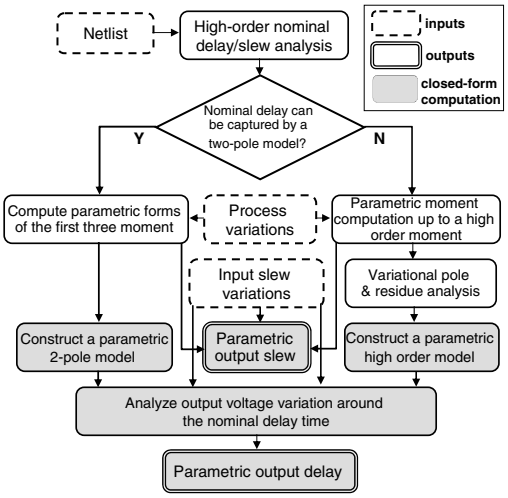

Figure 1: Variational delay and slew computation.

3. PARAMETRIC MOMENT ANALYSIS

An RC network with a single voltage input can be described using the following system equations

$$C\frac{dx}{dt} + Gx = bu,\ y = L^T x, \tag{2}$$

where $G, C \in \mathbf{R}^{N\times N}$ are the conductance and capacitance matrices, u is the voltage source, $x \in \mathbf{R}^{N\times 1}$ is the unknown vector consisting of the node voltages and the voltage source current, $b \in \mathbf{R}^{N\times 1}$ is a vector linking the input to the RC circuit, and $L \in \mathbf{R}^{N\times M}$ is the output matrix used to select the sink node voltages $y \in \mathbf{R}^{M\times 1}$ from x. Throughout this paper, the notation (G, C, b, L) is used to denote a single-input RC network commonly encountered in timing analysis.

Variations of G and C matrices are modeled by quadratic dependency on the process parameters ρ. Without loss of generality, we only consider a linear dependency for simplicity of notation as follows

$$G = G_0 + \sum_{i=1}^{N_\rho} G_i\rho_i,\ C = C_0 + \sum_{i=1}^{N_\rho} C_i\rho_i, \tag{3}$$

where G_i and C_i are sensitivity matrices and can be obtained during the parasitics extraction. The zero-th order moment of a RC network without any grounded resistance is given by $m^0 \in \mathbf{R}^{N\times 1}$ is given as $m^0 = G^{-1}b = [1\ 1\cdots 1\ 0]^T$ regardless of process variations. In the following, the quadratic parametric forms of the next three moments are derived.

The quadratic parametric form of the ith order moment $m^i \in \mathbf{R}^{N\times 1}$ vector is represented in the following form

$$m^i = m_0^i + \sum_{j=1}^{N_\rho} \alpha_j^i\rho_j + \sum_{j=1}^{N_\rho}\sum_{k=1}^{N_\rho} \gamma_{j,k}^i\rho_j\rho_k, \tag{4}$$

where m_0^i is the nominal value, $\alpha_j^i \in \mathbf{R}^{N\times 1}$ and $\gamma_{j,k}^i \in \mathbf{R}^{N\times 1}$ are the first and second order coefficients. Since circuit moments are computed recursively in an ascending order, it will suffice to show how the next moment vector m^{i+1} is computed given m^i. Assuming that the parametric form of m^i as in (4) is available, m^{i+1} can be obtained as

$$m^{i+1} = -G^{-1}Cm^i = -(G_0+\sum_{i=1}^{N_\rho} G_i\rho_i)^{-1}(C_0+\sum_{i=1}^{N_\rho} C_i\rho_i)m^i, \tag{5}$$

where the matrix inversion can be expanded using Taylor series since the perturbation term is assumed to be small

$$\begin{aligned}(G_0 + \sum_{i=1}^{N_\rho} G_i\rho_i)^{-1} &= \Big(I - \sum_{i=1}^{N_\rho} G_i\rho_i + (\sum_{i=1}^{N_\rho} G_i\rho_i)^2 \\ &\quad -(\sum_{i=1}^{N_\rho} G_i\rho_i)^3 + \cdots\Big)G_0^{-1}.\end{aligned} \tag{6}$$

Substituting (4) and (6) into (5) and retaining only up to the quadratic terms gives

$$m^{i+1} = m_0^{i+1} + \sum_{j=1}^{N_\rho} \alpha_j^{i+1}\rho_j + \sum_{j=1}^{N_\rho}\sum_{k=1}^{N_\rho} \gamma_{j,k}^{i+1}\rho_j\rho_k, \tag{7}$$

where

$$\begin{aligned} m_0^{i+1} &= -G_0^{-1}C_0m_0^i \\ \alpha_j^{i+1} &= G_0^{-1}G_jG_0^{-1}C_0m_0^i - G_0^{-1}C_0\alpha_j^i - G_0^{-1}C_jm_0^i \\ \gamma_{j,k}^{i+1} &= \gamma_{j,k}^{i+1,1} + \gamma_{j,k}^{i+1,2}. \end{aligned} \tag{8}$$

In (8), the second order coefficient $\gamma_{j,k}^{i+1}$ is split into two parts which are given by

$$\begin{aligned}\gamma_{j,k}^{i+1,1} &= -G_0^{-1}G_jG_0^{-1}G_kG_0^{-1}C_0m_0^i + G_0^{-1}G_jG_0^{-1}C_0\alpha_k^i \\ &\quad -G_0^{-1}G_jG_0^{-1}C_km_0^i - G_0^{-1}C_k\alpha_j^i,\end{aligned} \tag{9}$$

$$\gamma_{j,k}^{i+1,2} = -G_0^{-1} C_0 \gamma_{j,k}^i, \quad (10)$$

where the second order coefficient $\gamma_{j,k}^i$ (for $\rho_j \rho_k$) of m^i is defined recursively as in (8). For the zero-th order moment m^0, it is true that $\alpha_j^i = \gamma_{j,k}^0 = 0$.

A few key observations are due here. Starting from $m^0 = G^{-1}b = [1\ 1 \cdots 1\ 0]^T$, the parametric forms of the first few moments can be computed using (5, 8, 9, 10). As in (4), the N_ρ sensitivity vectors α_j^i's can be computed using the standard sensitivity analysis, achievable by reusing the LU factor of G_0 or applying path tracing (RICE [10]) with mild computational cost. The large number ($O(N_\rho^2)$) of second order coefficients are more expensive to compute in (4). To speedup, we exploit the observation: in a typical RC signal net, the number of sink nodes, N_s, is typically much less than the number of circuit unknowns N. Hence, efficiency of analysis can be improved if the second order analysis is only conducted for the sink nodes. In our implementation, the nominal moments and first-order sensitivity vectors are computed for all N circuit nodes while the second order coefficients are only computed for N_s sink nodes. As an example, let us consider the term in (10). Instead of computing the complete $\gamma_{j,k}^{i+1,2}$, we seek the entries of the sink nodes of interest. We multiply $\gamma_{j,k}^{i+1,2}$ with L^T ($L \in \mathbf{R}^{N \times N_s}$) from left to select just what corresponds to N_s sink nodes

$$L^T \gamma_{j,k}^{i+1,2} = -L^T G_0^{-1} C_0 \gamma_{j,k}^i = \Phi^T \gamma_{j,k}^i, \quad (11)$$

where $\Phi = -\Theta^T C_0$ and $\Theta = (G_0^T)^{-1} L$ is obtained via solving the adjoint linear system defined by G_0^T by reusing the same LU factor of G_0. Considering only N_s sink nodes changes the cost from $O(N_\rho^2)$ linear system solutions/matrix-vector multiplications to $O(N_s N_\rho^2)$ vector inner products. When N_s is small, the latter can be performed faster using vector operations. It should be noted in evaluating (11), vector $\gamma_{j,k}^i \in \mathbf{R}^{N \times 1}$ is not formed directly either since there exist also $O(N_\rho^2)$ of them. Instead, $\Phi^T \gamma_{j,k}^i$ is evaluated.

4. SLEW RATE COMPUTATION

The variation of the slew at any given sink node say, j, is analyzed based on the parametric moments computed in the previous section. Here, slew is computed on a per sink node basis, thus it only involves scalar computations while considering parametric variations. Unlike delay computation, there do exist simple moment-based slew metrics that are accurate for both the near and far end nodes [12, 13].

In [9], the PERI metric is used to estimate the sink node slew for a given input slew

$$slew_{ramp} = \sqrt{slew_{step}^2 + slew_{input}^2}, \quad (12)$$

where $slew_{input}$ is the slew of the ramp input, $slew_{step}$ is the output slew for a step input, and $slew_{ramp}$ is the output slew for the ramp input. It is shown that the above metric can correlate fairly accurately the ramp input slew with the output slew if an accurate metric for $slew_{step}$ is used. In this paper, it is assumed that the nominal output slew $slew_{ramp}^0$ has been accurately obtained. Then, the variation of $slew_{step}$ around $slew_{step}^0$ is estimated as

$$slew_{step} = \frac{m_j^1 \cdot slew_{step,0}}{m_{j,0}^1}, \quad (13)$$

where m_j^1 and $m_{j,0}^1$ are first order moment and its nominal value at the sink node j. In the above, the (variational) Elmore delay of the node is normalized with respect to the nominal slew to provide a variational step-input slew metric. Let us assume that the variational forms of $slew_{in}$ and $slew_{step}$ are cast into

$$slew_{in} = \alpha_i + \beta_i^T \rho + \rho^T \Gamma_i \rho,\ slew_{step} = \alpha_s + \beta_s^T \rho + \rho^T \Gamma_s \rho, \quad (14)$$

where α_i and α_s are scalars, β_i^T and β_s^T are $N_\rho \times 1$ vectors, Γ_i and Γ_s are $N_\rho \times N_\rho$ matrices. Substituting (14) into (12) and expanding about the nominal ramp-input output slew gives the following variational form of $slew_{ramp}$

$$slew_{ramp} = \sqrt{\alpha_s^2 + \alpha_s^2}(1 + \beta_r^T \rho + \rho^T \Gamma_r \rho), \quad (15)$$

where

$$\begin{aligned} \beta_r &= \frac{\alpha_i \beta_i + \alpha_s \beta_s}{\alpha_i^2 + \alpha_s^2} \\ \Gamma_r &= \frac{\beta_i \beta_i^T + \beta_s \beta_s^T + 2(\alpha_i \Gamma_i + \alpha_i \Gamma_i)}{2(\alpha_i^2 + \alpha_s^2)} - \frac{1}{8} \beta^T \beta_r^T . \end{aligned} \quad (16)$$

We have found in our experiments that the above variational slew metric is very accurate. It is also possible to use the two-moment slew metric proposed in [13]. The computation of the parametric form of the output slew can be similarly conducted.

5. VARIATIONAL DELAY ANALYSIS

Unlike the slew analysis, simple moment-based interconnect delay metrics tend to be inaccurate for near end nodes, making it not completely suitable for variation analysis. We propose to analyze the output voltage response variation at the nominal delay point (e.g. $50\%V_{dd}$ crossing point) and then convert the variation in response to variation in delay.

As shown in Fig. 1, each sink node is identified either as a "near" end node or a "far" end node by examining the results of the nominal analysis. For a "far" end node, a parametric two-pole AWE model is constructed to evaluate its voltage response variation while for a "near" end node, perturbation analysis of poles and residues is conducted to construct a more accurate parametric high-order AWE model. The strategy here is that majority of nodes (those are of far-end in nature) can be processed rather efficiently using simple two-pole models and a smaller number of near-end nodes are analyzed using high-order models. When using only the nominal analysis result to decide the nature of a sink node, we have assumed that process variations do not make a near-end node behave like a far-end node and vice versa. This is a quite reasonable assumption since for bounded process variations the nature of a circuit node is determined by its location. For an arbitrary sink node, let us assume that a set of N_r pole and residue pairs, $p_{nom,i}$ and $k_{nom,i}$ are computed in an accurate high-order AWE analysis used for the nominal case timing analysis. From this analysis, the nominal $50\%V_{dd}$ crossing time is assumed to be t_{nom}. Then, the portion of output response at time t_{nom} attributed to the two most dominant low frequency poles, say, $p_{nom,1}$ and $p_{nom,2}$, is computed as V_l. For a given user-specified tolerance ε ($\varepsilon < 1$), the sink node is identified as a far-end node if

$$|0.5V_{dd} - V_l| < 0.5\varepsilon V_{dd}. \quad (17)$$

Otherwise, it is identified as a near-end node.

5.1 Parametric two-pole model

We describe how a parametric two-pole model can be efficiently constructed for far-end nodes. A second order AWE model parameterizable in the same quadratic parametric form is computed. This goal can be achieved by propagating the parametric moment expressions derived in the

previous sections though the moment matching procedure. Since the order of moment matching is low, it is possible to derive closed-form formulas. As an example, let us consider the characteristic function of a 2nd order AWE model

$$b_2 p^2 + b_1 p + 1 = 0, \tag{18}$$

where b_1 is determined by the moment matching process using circuit moments as $b_1 = \frac{-m_0 m_3 + m_1 m_2}{m_0 m_2 - m_1^2}$. Notice that the parametric form of these moments can be computed using the procedure described in the previous sections. Denote the parametric expressions for the first four moments as

$$m_i = \alpha_{m,i} + \beta_{m,i}^T \rho + \rho^T \Gamma_{m,i} \rho, i = 0, 1, 2, 3. \tag{19}$$

Substituting (19) into (18) and keeping up to the 2nd order parametric terms gives

$$b_1 \approx \frac{f_1}{f_2}, \tag{20}$$

where

$$\begin{aligned} f_1 \;=\; & (\alpha_{m,1}\alpha_{m,2} - \alpha_{m,0}\alpha_{m,3}) + \\ & (\alpha_{m,1}\beta_{m,2}^T + \alpha_{m,2}\beta_{m,1}^T - \alpha_{m,0}\beta_{m,3}^T)\rho + \\ & \rho^T(\alpha_{m,1}\Gamma_{m,2} + \beta_{m,1}\beta_{m,2}^T + \alpha_{m,2}\Gamma_{m,1} - \alpha_{m,0}\Gamma_{m,3})\rho, \end{aligned} \tag{21}$$

$$\begin{aligned} f_2 \;=\; & (\alpha_{m,0}\alpha_{m,2} - \alpha_{m,1}^2) + (\alpha_{m,0}\beta_{m,2}^T - 2\alpha_{m,1}\beta_{m,1}^T)\rho + \\ & \rho^T(\alpha_{m,0}\Gamma_{m,2} - 2\alpha_{m,1}\Gamma_{m,1} - \beta_{m,1}\beta_{m,1}^T)\rho. \end{aligned} \tag{22}$$

Here, b_1 is in the form of a ratio of two quadratic forms. In our implementation, analytical expressions have been derived to convert such a ratio into a standard quadratic form. Going though similar derivations, b_2 as well as two pole/residue pairs of the two-pole model, k_1, p_1, k_2, p_2, can be obtained in the same parametric quadratic form. Essentially, by passing parametric moments to a set of pre-stored closed-form formulas, a parametric two-pole model can be computed very efficiently for any given circuit node.

5.2 Parametric high-order AWE model

For sinks that are identified as near-end nodes, a two-pole model is not accurate enough to analyze the variation in the voltage response. Instead, we seek an accurate parametric high-order AWE model. The order of parametric model can be set to what is used in the nominal case timing analysis. Unlike a simple two-pole model, it is not possible to derive closed-form expressions to relate the circuit moments to a high order model. Hence, we first numerically compute the parametric variations of the characteristic function of the AWE model and then perform perturbation analysis on system poles and residues to produce the desired parametric model. Without loss of generality, consider the correspondence between the circuit moments and the coefficients of the characteristic function in a 4-th order AWE model

$$\begin{bmatrix} m_0 & m_1 & m_2 & m_3 \\ m_1 & m_2 & m_3 & m_4 \\ m_2 & m_3 & m_4 & m_5 \\ m_3 & m_4 & m_5 & m_6 \end{bmatrix} \begin{bmatrix} b_4 \\ b_3 \\ b_2 \\ b_1 \end{bmatrix} = - \begin{bmatrix} m_4 \\ m_5 \\ m_6 \\ m_7 \end{bmatrix}. \tag{23}$$

To simplify the notation, we denote the Hankel matrix in the above equation as F, its nominal matrix as F_0, its first sensitivity w.r.t the i-th process variable ρ_i as F_i and its second order dependency on $\rho_i \rho_j$ as $F_{i,j}$. Notice that F_i and $F_{i,j}$ can be obtained by replacing each moment in F by its first order sensitivity w.r.t ρ_i and second order dependency w.r.t $\rho_i \rho_j$, respectively. We further denote $[b_4\ b_3\ b_2\ b_1]^T$ as $\mathtt{b}$, $[m_4\ m_5\ m_6\ m_7]^T$ as $\mathtt{m}$, and their nominal values as $\mathtt{b_0}$ and $\mathtt{m_0}$, respectively. We define $\mathtt{b_i}$, $\mathtt{m_i}$, $\mathtt{b_{i,j}}$ and $\mathtt{m_{i,j}}$ as in the case of F. A standard sensitivity analysis gives

$$\mathtt{b_i} = F_0^{-1}(-\mathtt{m_i} - F_i \mathtt{b_0}). \tag{24}$$

Matching the second order terms from the both sides of (23) leads to

$$\mathtt{b_{i,j}} = F_0^{-1}(-\mathtt{m_{i,j}} - F_i \mathtt{b_j} - F_{i,j} \mathtt{b_0}). \tag{25}$$

Using the parametric moments already computed, the parametric forms of $\mathtt{b}$ can be obtained by solving multiple linear matrix problems defined by the nominal Hankel matrix.

With the parametric dependency of the characteristic function (defined by $\mathtt{b}$) computed, we proceed to analyze the variation of the system poles. For general high-order models, no closed-form expressions are available for poles. To make the problem of analyzing parametric variations of transfer function poles tractable, perturbation analysis is applied in the neighborhood of each nominal model pole, as illustrated in Fig. 2. To capture the variation of a pole of the high-order AWE model around its nominal value, say $p_{nom,i}$, the characteristic function

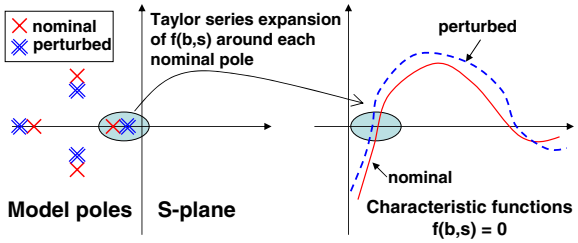

Figure 2: Perturbation analysis of model poles.

$$f(\mathtt{b}, s) = 1 + b_1 s + b_2 s^2 + b_3 s^3 + b_4 s^4 = 0 \tag{26}$$

is expanded into a quadratic function at $s = p_{nom,i}$ as

$$f(\mathtt{b}, \Delta p_i) = q_0 + q_1 \Delta p_i + q_2 \Delta p_i^2 = 0, \tag{27}$$

where, Δp_i is the variation of the i-th pole and

$$\begin{aligned} q_0 \;&=\; 1 + b_1 p_{nom,i} + b_2 p_{nom,i}^2 + b_3 p_{nom,i}^3 + b_4 p_{nom,i}^4 \\ q_1 \;&=\; b_1 + 2b_2 p_{nom,i} + 3b_3 p_{nom,i}^2 + 4b_4 p_{nom,i}^3 \\ q_2 \;&=\; b_2 + 3b_3 p_{nom,i} + 6b_4 p_{nom,i}^2. \end{aligned} \tag{28}$$

Notice that since $\mathtt{b}$ has parametric variations, q_0 in (28) is not necessarily zero. Using the parametric expressions of $\mathtt{b}$, $q_i's$ in the above equation can be cast in the following quadratic forms in the process variables

$$q_i = q_{i,0} + q_{i,1}^T \rho + \rho^T Q_{i,2} \rho \tag{29}$$

Plugging $\Delta p_i = p_{i,1}^T \rho + \rho^T P_{i,2} \rho$ into (27) gives

$$p_{i,1} = -q_{0,1}/q_{1,0},\ P_{i,2} = -(q_{0,2} + q_{1,1} p_{i,1}^T + q_{2,0} p_{i,1} p_{i,1}^T)/q_{1,0}. \tag{30}$$

After the perturbation analysis is completed for all poles, the resulting parametric expressions are employed to compute the parametric forms of residues ($k_i's$) that leads to a complete parametric circuit model. Given a N_m-th order parametric model, the variation of the time-domain voltage response $y(t)$ at any time t under a saturated ramp input can be evaluated using

$$\begin{aligned} y(t) \;=\; & \sum_{i=1}^{N_m} \frac{a k_i}{p_i^2} \big[(-1 - p_i t + e^{p_i t})U(t) - \\ & (-1 - p_i(t - t_1) + e^{p_i(t-t_1)})U(t - t_1)\big], \end{aligned} \tag{31}$$

where a is the slope of the ramp input, $t_1 = V_{dd}/a$, and $U(\cdot)$ is the step function. Utilizing the parametric poles/residues, expanding $y(t)$ around its nominal value leads to a second order parametric expression of the voltage response.

6. DELAY VARIATION

In the nominal case delay analysis, typically, a reduced order model is computed to obtain the analytical solution of the voltage response at a sink node under the saturated ramp input. To find the output delay, nonlinear Newton iterations are applied to find the time t_{nom} at which the output voltage crosses $50\%V_{dd}$. However, applying nonlinear iterations over a large number of circuit instances to find the delay variation is prohibitively expensive. To facilitate a feasible variational delay analysis, in our approach, we convert the variation in the output response at t_{nom}, namely, ΔV, to the variation in delay. As shown in Fig. 3, the rationale behind is that although finding a particular voltage crossing point is intrinsically difficult, evaluating variation of the response at a given time is rather straightforward. The latter is achieved by using the parametric two-pole or high-order AWE model developed in the previous sections.

To this end, two fixed time points t_a and t_b are selected

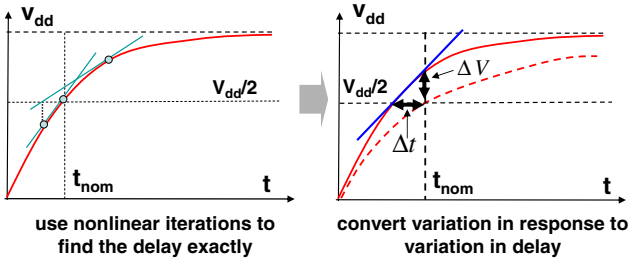

Figure 3: Avoiding nonlinear iterations by converting voltage response variation to delay variation.

in the neighborhood of t_{nom}: $t_a < t_{nom} < t_b$. The voltage response at these two points can be similarly obtained from the parametric model computed previously. The slope of the voltage response around t_{nom} can be approximated as

$$slope(t_{nom}) = \frac{y(t_b) - y(t_a)}{t_b - t_a}. \quad (32)$$

Using (32), the delay variation is estimated as

$$t_d = t_{nom} - \frac{\Delta V(t_b - t_a)}{y(t_b) - y(t_a)}, \quad (33)$$

which can be finally converted to a standard quadratic parametric form. It should be noted that in (33) the variation of $slope(t_{nom})$ is also reflected in the delay variation.

7. EXPERIMENTAL RESULTS

We first demonstrate the accuracy issue of variational interconnect analysis using two circuit examples. In Fig. 4(a), a ramp input is applied to a RC circuit and a far end node is selected to examine the voltage response. We compare the direct transient simulation and the 2nd order AWE model for the original circuit and the perturbed circuit where RC values are varied to mimic the impact of process variation. As can be seen, for this far end node the 2nd order AWE model is very accurate for both the original circuit and the perturbed one. Therefore, it is well expected that delay/slew variation can be accurately captured if a parametric 2nd order AWE model is extracted. We conduct a similar comparison for a near end node selected from another RC circuit in Fig. 4(b). This near end node is located close to the driving voltage input therefore resistive shielding effect is noticeable in this case. It is clearly seen that the 2nd order AWE model cannot capture well the variation of the output response. However, a 4th order model can. This implies that for near end nodes, delay/slew variations cannot be well captured by a low order model. For a case like this, the perturbation analysis will be invoked in the proposed variational analysis flow to produce a high-order parametric model to ensure the accuracy.

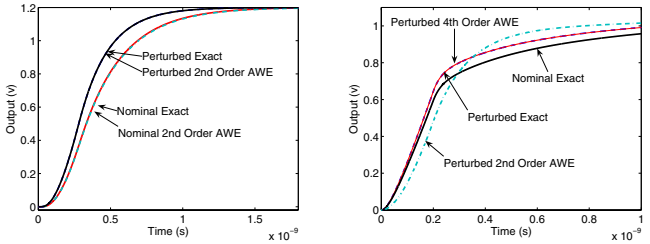

(a) Far end node (b) Near end node

Figure 4: Nominal and variational analysis for a far-end and near-end node.

Next, we demonstrate the accuracy of the proposed analysis on a near-end node chosen from a RC circuit with 124 nodes and 234 RC elements, as shown in Fig. 5. This circuit is driven by a saturated ramp signal with a nominal input slew rate of 200ps. 10 independent RC variation sources are considered so is the variation in the input slew. In practice, near end nodes are usually difficult to estimate using moment-based delay metrics. However, in the proposed technique, this node is identified to be a near-end node in the nominal case timing analysis. When performing the variational analysis, the perturbation analysis is invoked to generate a 4-th order parametric AWE model and the quadratic parametric forms are computed for delay and slew. 500 circuit samples are randomly generated and we directly compute the output delay and slew of each sample by applying transient analysis. For comparison, the parametric delay and slew expressions obtained from our proposed technique are evaluated for these 500 circuit samples. In Fig. 5, the relative errors of delay and slew of the proposed variational technique are shown. In this case, the maximum errors are 4.2% and 2.7% for delay and slew, respectively.

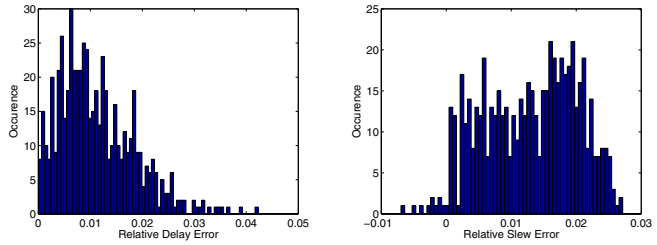

(a) Relative Delay Error (b) Relative Slew Error

Figure 5: Error distributions for an near-end node.

Next, we examine the statistical distributions of the interconnect delay and slew in a RC circuit. For this case, 10 independent process parameters are considered and a fixed ramp input with a 50ps slew is applied to each circuit instance. The PDFs of the delay and the slew at one circuit node are examined in Fig. 6. As clearly seen from the fig-

ure, the PDFs of our variational analysis match very well with those computed by the corresponding 8-th order AWE model for each case.

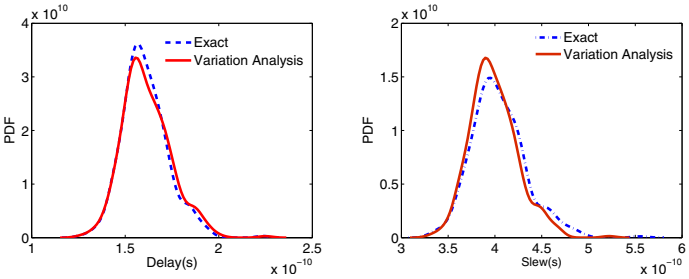

(a) PDF of the delay. (b) PDF of the slew.

Figure 6: PDFs of delay and slew of a node.

For more extensive verification of the proposed techniques, we consider a set of RC nets with different sizes ranging from a few ten nodes to a few hundred nodes and several hundred circuit elements, in Table 1. and Table 2. For each circuit, a circuit node is arbitrarily chosen as one sink node for comparison. Again, 10 independent process parameters are considered which are perturbed with various degrees to generate 500 samples for each circuit. In Table 1, the input to all the nets is a fixed ramp input with 50ps slew rate while the input in Table 2 has a nominal slew of 200ps and varies with the same 10 process parameters. In the second columns of the both tables, the maximum percentages of delay and slew variations (with respect to the nominal values) seen across the 500 samples are listed to indicate the degree of variability. In both tables, we list the maximum and average relative errors for delay and slew for each of these circuits and compare the 2nd-order parametric analysis (5th/6th columns) with the first-order sensitivity analysis (3rd/4th columns). As a reference, a high order AWE model and nonlinear iterations are applied to compute the delay and slew for each sample, which are regarded as the exact solution. In the table, "-" indicates the cases where the corresponding analysis generates a significant error in estimating delay or slew. It can be clearly seen from these tables that for a wide range of delay/slew variations, the presented 2nd-order parametric analysis can maintain very good accuracy. It should be noted that for some cases, the first-order analysis completely fails to capture the large variability.

8. CONCLUSIONS

In this paper, a practical variation-aware methodology is presented to analyze interconnect performance variations. Specific techniques have been developed such that a 2nd-order parametric analysis can be done efficiently for on-chip RC interconnects for a large number of process variations manifesting in terms of RC value perturbations and input slew variations. The proposed variational analysis can accurately capture wide variations of interconnect delay and slew even under the cases where the simpler first-order sensitivity analysis completely fails. Since the proposed technique produces parametric expressions for delay and slew, it is expected that the the technique and its extensions can be incorporated easily into a statistical timing environment as an interconnect delay calculator.

9. REFERENCES

[1] L. Pillage and R. Rohrer. Asymptotic waveform evaluation for timing analysis. *IEEE Trans. Computer-Aided Design*, 9:352–366, April 1990.

[2] S. Nassif. Modeling and analysis of manufacturing variations. In *Proc. IEEE Custom Integrated Circuits Conf.*., pages 223–228, 2001.

[3] L. Daniel, O. Siong, L. Chay, K. Lee, and J. White. A multi-parameter moment-matching model-reduction approach for generating geometrically parameterized interconnect performance models. *IEEE Trans. Computer-Aided Design*, 23(5):678–693, May 2004.

[4] P. Li, Y. Liu, X. Li, L. Pileggi, and S. Nassif. Modeling interconnect variability using efficient parametric model order reduction. In *Proc. IEEE/ACM DATE*, March 2005.

[5] K. Agarwal, D. Sylvester, D. Blaauw, F. Liu, S. Nassif, and S. Vrudhula. Variational delay metrics for interconnect timing analysis. In *Proc. IEEE/ACM DAC*, June 2004.

[6] J. Wang, P. Ghanta, and S. Vrudhula. Stochastic analysis of interconnect performance in the presence of process variations. In *Proc. IEEE/ACM ICCAD*, pages 880–886, November 2004.

[7] C. Visweswariah, K. Ravindran, K. Kalafala, S. Walker, and S. Narayan. First-order incremental block-based statistical timing analysis. In *Proc. IEEE/ACM DAC*, June 2004.

[8] C.Alpert, A. Devgan, and C. Kashyap. Rc delay metrics for performance optimization. *IEEE Trans. Computer-Aided Design*, 20:571–582, May 2001.

[9] C. Kashyap, J. Alpert, F. Liu, and A. Devgan. Closed-form expressions for extending step delay and slew metrics to ramp inputs for rc trees. *IEEE Trans. Computer-Aided Design*, 23, April 2004.

[10] C. Ratzlaff and L. Pillage. Rice: rapid interconnect circuit evaluation using awe. *IEEE Trans. Computer-Aided Design*, 13(6):763–776, June 1994.

[11] Y. Zhan, A. Strojwas, X. Li, and L. Pileggi. Correlation-aware statistical timing analysis with non-guassian delay distributions. In *Proc. IEEE/ACM DAC*, June 2005.

[12] H. B. Bakoglu. *Circuits, interconnections and packaging for VLSI*. Addison-Wesley, Reading, MA, 1990.

[13] K. Agarwal, D. Sylvester, and D. Blaauw. Simple metrics for slew rate of rc circuits based on two circuit moments. In *Proc. IEEE/ACM DAC*, June 2003.

Table 1: Variational interconnect analysis results: fixed input slew (50ps)

Net	Max D/S Var.%	1st: Max/Ave%		2nd: Max/Ave%	
		Delay E.	Slew E.	Delay E.	Slew E.
1	34.6/36.8	81.0/7.0	17.1/2.2	2.8/0.9	11.1/1.1
2	59.5/64.7	49.3/8.5	23.5/2.4	2.2/0.7	13.1/1.1
3	31.2/33.8	32.8/6.2	15.4/2.3	5.2/0.9	8.5/0.9
4	45.9/49.7	33.1/8.3	14.5/2.9	3.4/0.9	6.9/1.0
5	61.9/62.1	93.7/16.0	-/-	5.0/1.1	4.2/0.5
6	61.1/62.2	98.6/16.2	-/-	6.3/1.1	4.4/0.5
7	29.6/31.3	37.8/5.5	10.0/1.8	2.7/0.8	3.0/0.7
8	17.6/17.1	32.3/4.2	5.5/1.0	2.5/0.7	2.4/0.6
9	26.7/28.1	9.4/3.1	11.3/13.2	3.4/0.5	4.6/0.8
10	27.9/29.2	11.1/3.4	11.9/3.3	3.2/0.4	3.8/0.7
11	31.7/35.8	19.0/3.9	19.8/3.9	7.1/0.5	9.6/0.9
12	40.6/41.9	16.5/3.9	19.7/3.7	6.3/0.8	10.6/0.9
13	50.9/47.7	20.3/2.9	18.8/2.7	8.0/0.5	8.5/0.6
14	27.3/29.7	17.2/3.5	18.8/3.3	5.7/0.6	7.2/0.8
15	21.7/23.2	13.3/3.6	47.9/3.4	3.0/0.6	5.3/0.9
16	32.9/33.0	14.6/3.6	14.0/3.3	3.9/0.5	4.1/0.7

Table 2: Variational interconnect analysis results: w/ input slew variations (nominal slew 200ps)

Net	Max D/S Var.%	1st: Max/Ave%		2nd: Max/Ave%	
		Delay E.	Slew E.	Delay E.	Slew E.
1	30.9/28.5	43.9/5.5	9.9/2.4	3.47/0.5	5.7/1.3
2	46.9/32.1	48.8/6.9	9.2/1.4	3.8/0.4	6.4/1.3
3	21.9/19.2	24.7/4.3	8.7/2.9	2.7/0.8	4.6/1.5
4	12.5/13.5	15.6/4.3	4.8/1.2	2.3/0.7	2.1/0.6
5	76.7/93.6	59.9/10.1	-/-	6.9/1.3	5.0/4.6
6	79.1/13.8	6.9/10.0	-/-	7.4/1.1	7.2/6.0
7	18.9/19.0	28.8/5.3	8.0/2.9	3.1/0.6	4.3/1.5
8	16.3/16.4	25.1/4.0	8.1/2.2	2.3/0.5	3.1/1.3
9	55.9/49.5	18.1/3.4	12.1/2.4	7.8/1.8	6.9/3.1
10	27.4/22.7	9.7/0.8	5.8/1.7	3.6/1.3	5.8/2.8
11	32.6/42.7	14.0/1.7	15.7/2.0	5.9/2.1	11.0/2.1
12	11.6/12.1	4.1/0.6	3.6/0.9	2.6/0.5	2.7/1.2
13	17.3/16.8	5.1/0.7	4.4/0.8	2.5/0.6	3.2/1.3
14	33.0/35.1	9.0/1.2	6.8/1.0	4.4/1.2	3.5/1.5
15	37.9/29.4	9.4/1.4	9.2/1.1	4.9/1.3	4.3/1.4
16	36.4/34.0	8.1/1.1	5.7/1.0	4.2/1.1	2.7/1.3